



Cite this: *Chem. Sci.*, 2025, **16**, 19702

All publication charges for this article have been paid for by the Royal Society of Chemistry

Received 26th June 2025
Accepted 19th September 2025

DOI: 10.1039/d5sc04731e
rsc.li/chemical-science

Introduction

Carbon capture is an attractive strategy for mitigating anthropogenic CO₂ emissions to curb global climate change. Developing this technology is especially important for sectors where emissions are hard to abate through other means, such as the cement or steel industry. Currently, most deployed carbon capture systems rely on liquid sorbents that must be thermally regenerated when saturated.¹ This energy-consuming step substantially raises operational costs, thus presenting a barrier to the widespread adoption of the technology. In addition, the regeneration step has a large CO₂ footprint, thus partially offsetting the benefits of the capture process.² As such, developing more sustainable approaches to carbon capture is a timely challenge.

Recently, carbon capture methods relying on electrochemical regeneration have garnered significant attention as sustainable, efficient, and safe alternatives to the traditional thermal approach.¹⁻³ In many of these methods, low-cost electricity is used to reversibly interconvert a molecular redox mediator between two redox states, where one state leads to CO₂ capture while the other leads to CO₂ release.

Water-soluble pyridinium redox mediators for pH-swing CO₂ capture

Eloi Grignon,^{†a} Zhangfei Su,^{†c} Jiang Tian Liu,^a Armando Lima,^c Andrew Wang,^c Parisa Karimi,^c Shuai Chen^{*c} and Dwight S. Seferos^{†d}^{ab}

Electrochemical pH-swing processes offer a promising route for energy-efficient CO₂ capture but require robust redox mediators. This paper reports three water-soluble 4-substituted pyridinium redox mediators (BzM, BzSP, AcSP) for electrochemical pH-swing carbon capture and systematically evaluates their performance through H-cell and flow cell configurations. Highly water-soluble mediators bearing a propylsulfonate group can be readily synthesized in one step on a 20 g scale. We find that the inclusion of a benzoyl group at the 4-position is critical for attaining high current densities. The zwitterionic BzSP exhibits around 90% CO₂ capture efficiency and optimal CO₂ capture capacity (102 kJ mol_{CO₂}⁻¹) in a flow cell. These findings establish molecular design principles for pyridinium-based mediators in energy-efficient carbon management.

In the simplest redox-mediated electrochemical approach, direct binding, an initially unreactive mediator is reduced to a more nucleophilic state where it can temporarily bind electrophilic CO₂.⁴ Upon reoxidation of the mediator, its nucleophilicity is lowered and CO₂ is released. This strategy has been demonstrated in non-aqueous media with disulfides,⁵ pyridines,⁶ and quinones.⁷ However, in this method, the use of organic solvent as the electrolyte is undesirable from a cost and safety standpoint. A more elaborate approach, pH-swing, involves the reversible switching of the mediator's basicity through proton-coupled electron transfer (PCET).⁸ The principle of pH-swing CO₂ capture/release is illustrated in Fig. 1A. The reduction of the redox mediator consumes protons in the electrolyte, causing an increase in the electrolyte pH and the capture of CO₂ as carbonate or bicarbonate. Upon reoxidation, the mediator releases protons, leading to a decrease in the electrolyte pH and the release of CO₂. A key advantage of the pH-swing strategy is that the capture/release process occurs in water, which reduces operational costs, increases the system's safety, and enables high current densities. Several pH-swing mediator motifs have been reported, such as quinones,^{9,10} phenazines,¹¹⁻¹⁵ 1-aminopyridinium,¹⁶ riboflavin,¹⁷ and guanidines.¹⁸ However, the field is still nascent, and the exploration of further molecules is critical to enlarging the library of viable mediators.

Herein, we report pH-swing carbon capture based on 4-substituted acylpyridinium mediators. These molecules are synthesized in 1-2 steps and are isolated through a simple filtration, which is ideal for scale-up. The acylpyridinium molecular family was previously investigated for aqueous redox flow batteries by Sevor *et al.* and found to induce pH changes

^aDepartment of Chemistry, University of Toronto, Lash Miller Chemical Laboratories, 80 St. George Street, Toronto, Ontario, M5S 3H6, Canada

^bDepartment of Chemical Engineering and Applied Chemistry, University of Toronto, 200 College Street, Toronto, Ontario, M5S 3E5, Canada. E-mail: dwight.seferos@utoronto.ca

^cClean Energy Innovation Research Centre (CEI), National Research Council Canada, 2620 Speakman Drive, Mississauga, Ontario, L5K 2L1, Canada. E-mail: shuai.chen@nrc-cnrc.gc.ca

[†] These two authors contributed equally.



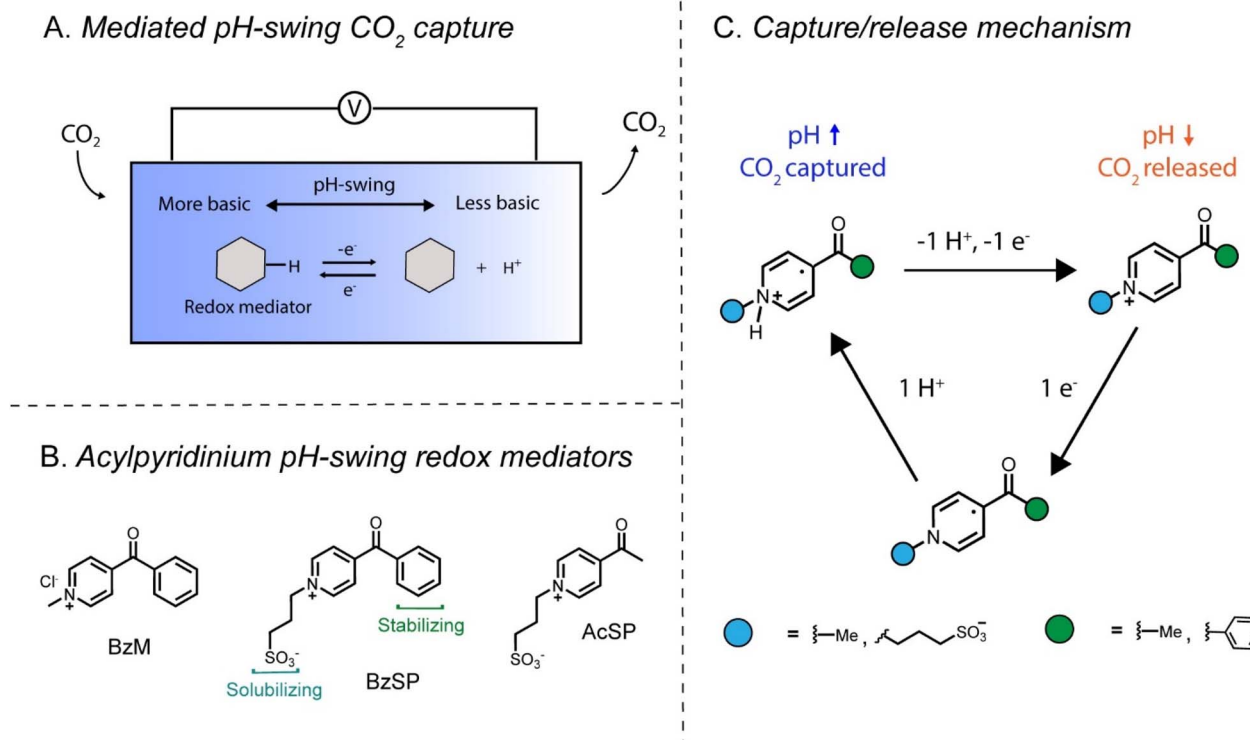


Fig. 1 (A) General scheme for redox-mediated pH-swing carbon capture in one compartment. (B) Acylpyridinium redox mediators used in this work. (C) Mechanism of CO_2 capture with pyridinium mediators.

due to proton abstraction.¹⁹ In this work, we exploit this property to mediate cyclical CO_2 capture.

The pyridinium mediators are synthesized in their oxidized form and can be reduced through PCET to form stable radicals. The solubility and radical stability of the mediators can be influenced by the group at the *N*- and 4-positions, respectively. In this study, we synthesized and studied three mediators: 4-benzoyl-1-methylpyridinium chloride (BzM), 3-(4-benzoylpyridin-1-ium-1-yl)propane-1-sulfonate (BzSP), and 3-(4-acetylpyridin-1-ium-1-yl)propane-1-sulfonate (AcSP) (Fig. 1B). The proton-coupled redox behavior of the mediators and their CO_2 capture/release mechanism is illustrated in Fig. 1C. During reduction, a pyridinium radical is formed, which takes up protons from the solution and enables CO_2 capture. In the subsequent reoxidation stage, the pyridinium radical undergoes electron loss and deprotonation, triggering CO_2 release. Overall, the mediators lower the energetic input required to generate a pH-swing, thus enabling energy-efficient CO_2 capture.

Results

CVs of pyridinium redox mediators

Cyclic voltammetry (CV) in 1 M KNO_3 (aq.) was used to screen the pH-swing mediators' electrochemical properties before capture/release tests. We started our exploration of this family of molecules with the previously reported BzM (Fig. 1B).^{19,20} A conservative potential window was employed to limit the

mediators to one reduction, thus avoiding the known reversibility issues associated with further reduced acylpyridinium products (Fig. S8).¹⁹ The redox process of BzM was first studied in solutions of varying pH to understand the influence of pH on reversibility and redox potential. The redox process is reversible at pH values above 11 but not at pH values below 10 (Fig. 2A), which implies a chemical step (protonation) when the concentration of H^+ is sufficiently high (*i.e.* when $\text{pH} < \text{p}K_{\text{a}}$). Moreover, CVs over a wide pH range show that the potential of BzM's first reduction is pH-dependent, with a change of approximately -49 mV pH^{-1} , confirming a $1 \text{ e}^-/1 \text{ H}^+$ proton-coupled electron transfer (Fig. 2B).²¹ This is consistent with a previous study of BzM.²⁰ Taken together, these findings confirm that BzM can be electrochemically transformed into a base, which is the fundamental requirement of a pH-swing mediator.

A high mediator solubility in all redox stages is important to maximize the capture solution's CO_2 capacity. BzM's solubility comes primarily from its positive charge, which disappears during the reduction step (unless protonated). Thus, to avoid possible solubility issues with BzM, we also synthesized BzSP, which bears a permanently anionic propylsulfonate group (Fig. 1B). These substituents have been used extensively as solubilizing groups for bispyridiniums (*i.e.* viologens) in aqueous redox-flow batteries.^{22–26} Finally, AcSP was synthesized as a control mediator to evaluate the influence of the substituent at the 4-position (Fig. 1B). All mediators showed the expected signals in their NMR (Fig. S1–S6) and FTIR (Fig. S7) spectra. In unbuffered 1 M KNO_3 (aq.), a clear redox event is

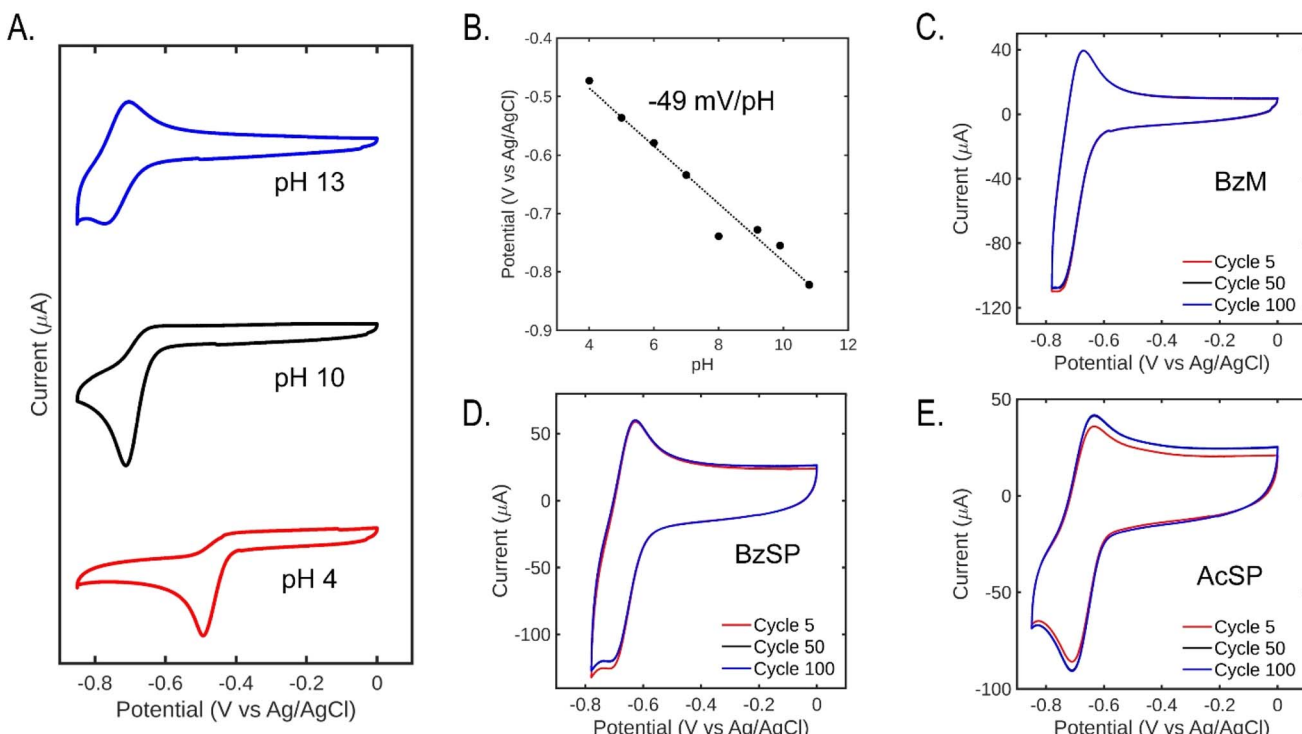


Fig. 2 Cyclic voltammetry of 5 mM pyridinium mediators at 100 mV s^{-1} under argon. (A) Cyclic voltammograms of BzM in various buffers with 1 M KNO_3 . (B) Pourbaix diagram of BzM. (C–E) Long-term cyclic voltammograms in unbuffered 1 M KNO_3 of BzM, BzSP, and AcSP.

observed at -0.71 V vs. Ag/AgCl for BzM and -0.69 V for BzSP and AcSP (Fig. 2C–E). The reduction of pyridinium mediators occurs within the pyridinium ring, and this structural feature is consistent in the three molecules, hence, the reduction potentials are similar. Prolonged CV experiments show slight variations in current in the early cycles, which is likely a result of local pH changes. However, the redox process quickly stabilizes and remains unchanged for at least 100 cycles. Finally, the reduction potentials of BzSP and AcSP also exhibit a strong pH-dependence, confirming the presence of PCET in these mediators (Fig. S9).

Carbon capture/release experiments in H-cell

Carbon capture/release experiments were carried out in an H-cell system (Fig. S10). The working electrode (WE) compartment contained 0.1 M pyridinium mediator and 1 M KNO_3 , while the counter electrode (CE) compartment contained 0.1 M $\text{K}_3\text{Fe}(\text{CN})_6$ and 0.2 M $\text{K}_4\text{Fe}(\text{CN})_6$, which served as an auxiliary redox couple. Pt coils were employed as WE and CE, with a Ag/AgCl (sat. KCl) as the reference electron (RE), which was located in the WE compartment. A pH sensor and CO_2 sensor provided real-time data on the capture/release process. Throughout the experiment, the solution in the WE compartment was continuously purged with a $\text{CO}_2 : \text{N}_2$ mixture (10 : 90, v/v), which simulates an industrial flue gas stream. A CO_2 concentration in the gas outlet lower than 10% corresponds to CO_2 capture, while CO_2 concentrations in the gas outlet higher than 10% indicate CO_2 release. In the test of BzSP and AcSP, the WE and CE compartments were separated by a Nafion 117 cation

exchange membrane (CEM), which allows cation transport between the two compartments during the test. However, since BzM is a cation, prolonged experiments result in its migration across the CEM to the CE compartment. This crossover phenomenon causes progressive depletion of BzM in the working electrolyte, ultimately diminishing the CO_2 capture capacity. Hence, in the test of BzM, a Fumasep FAA-3-PK-75 anion exchange membrane (AEM) was used to assemble the H-cell, and the electrolyte in the CE compartment comprised 0.2 M FeCl_2 and 0.1 M FeCl_3 .

Fig. S11 plots the CVs of three pyridinium mediators measured in the H-cell. The reduction current of BzM and BzSP is larger than AcSP, which follows the same trend as the CVs measured in diluted solution using the GC electrode, indicating that stabilizing benzoyl moiety facilitates electron transfer kinetics by increasing the stability of the reduction product. The reduction potential of BzSP (-0.78 V) is more positive compared to AcSP (-0.82 V) and BzM (-0.85 V with Nafion membrane), which is also in the same trend as the results in a diluted solution.

Fig. 3A plots the results of the CO_2 capture/release test using BzM as the redox mediator in the H-cell. During the experiment, the mediator was first reduced to generate a base, thus taking up protons from the solution and raising the pH. During this stage, acidic CO_2 was captured by the solution and stored as (bi) carbonate ions. Based on the CV (red curve in Fig. S11A) measured in the H-cell, the reduction potential for BzM was set at -0.90 V vs. Ag/AgCl . This potential was strategically set below the reduction potential of BzM, and above the hydrogen

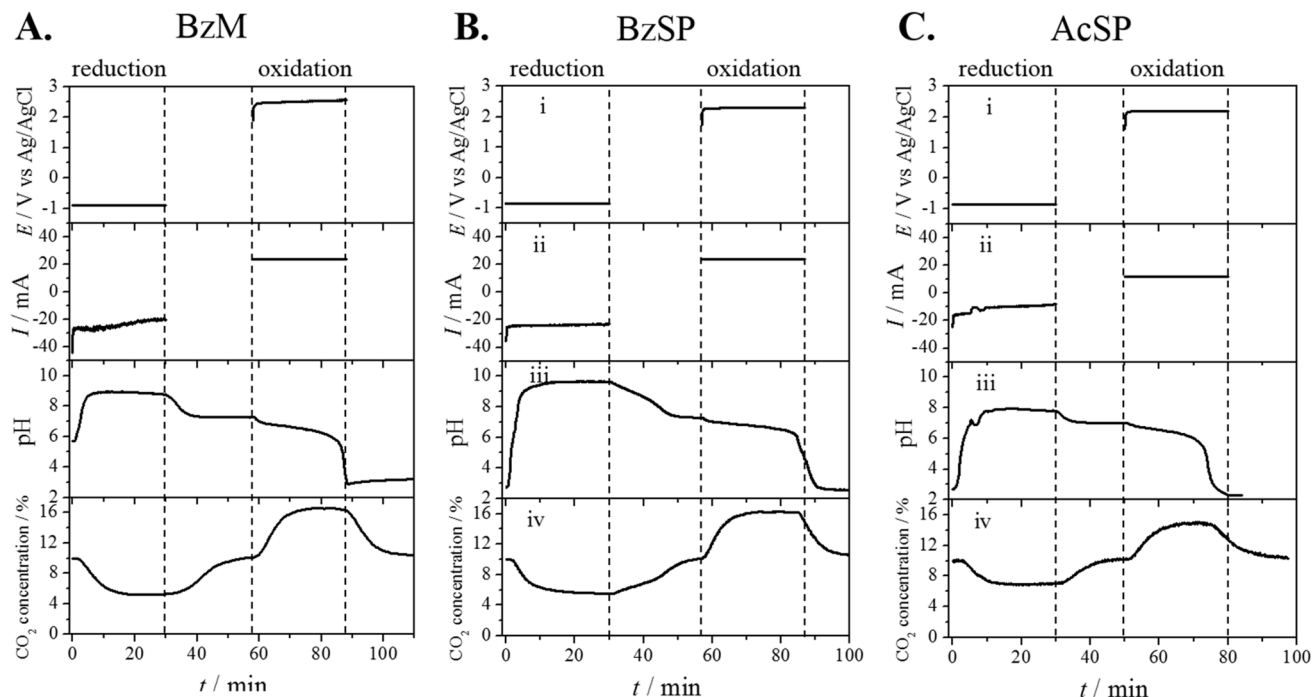


Fig. 3 H-cell CO_2 capture/release tests. (A–C) CO_2 capture/release results in the H-cell, (A) BzM, (B) BzSP, (C) AcSP. Fumasep AEM was used for BzM, and Nafion CEM was employed in the test of BzSP and AcSP. The pyridinium mediators were reduced using a constant potential and were reoxidized using a constant current. (i) Applied potential on the Pt WE, (ii) current of the Pt WE, (iii) pH of electrolyte in the WE compartment and (iv) CO_2 concentration in the gas outlet.

evolution reaction (HER) potential on the Pt surface, thereby suppressing competitive H_2 generation on the Pt coil. In Fig. 3A, the BzM reduction current was approximately -24.0 mA , accompanied by a gradual pH increase in the electrolyte. After 30 minutes of reduction, the potential was held at open circuit for 30 minutes to facilitate complete CO_2 capture. The solution pH decreased to 7.3 during this additional invasion period.

BzM was subsequently reoxidized under constant-current conditions at 24.0 mA , matching the average BzM reduction current. This condition ensured that the total charge passed through the Pt WE during the reduction and oxidation stages was balanced. The potential during BzM reoxidation was around $+2.5\text{ V}$ vs. Ag/AgCl , demonstrating that the reoxidation process is energetically demanding and requires external energy input. Concurrent with reoxidation, the pH within the WE compartment underwent a pronounced decrease, falling from 7.3 to 2.9. This acidification of the electrolyte enabled the efficient release of captured CO_2 from the solution. However, after the test, it was found that the OH^- anions generated in the reduction stage migrated across the AEM and formed $\text{Fe}(\text{OH})_2$ and $\text{Fe}(\text{OH})_3$ precipitates in the CE compartment. Hence, BzM is not a good candidate for the pH-swing CO_2 capture/release.

Fig. 3B and C show the results of the CO_2 capture/release test using BzSP and AcSP as the redox mediators. Based on the CVs (Fig. S11B & C) measured in the H-cell, the reduction potentials for BzSP and AcSP were set at -0.85 and -0.90 V vs. Ag/AgCl , respectively. The average BzSP reduction current was -23.9 mA , higher than AcSP's -12.0 mA . Following 30 minutes of reduction, the potential was held at open circuit for 30 minutes

to ensure complete CO_2 capture and proton regeneration. The mediators were then reoxidized in constant-current mode using currents equal to the absolute values of their respective reduction currents. BzSP demonstrates a better CO_2 capture capacity compared to AcSP, as evidenced by three key metrics: (1) a larger current in the reduction stage, (2) a more alkaline post-reduction solution (pH 9.7 for BzSP vs. 7.9 for AcSP), and (3) greater CO_2 concentration change in the gas outlet. These collective findings, as systematically demonstrated in Fig. 3B and C, establish BzSP's higher capacity in the pH-swing CO_2 capture system. The amplified pH fluctuation and corresponding gas concentration changes directly correlate with its improved charge transfer efficiency.

To distinguish whether CO_2 capture originates from the reduction of the pyridinium mediators or competing HER, a control experiment was performed in the H-cell containing exclusively 1 M KNO_3 in the WE compartment. Fig. S12A presents the carbon capture result obtained at a reduction potential of -0.85 V , which matches the potential applied for BzSP. The reduction current of 1 M KNO_3 without pyridinium mediator is between 1 and 2 mA, significantly lower than that observed in the electrolyte with 0.1 M BzSP , indicating that HER is quite slow at this potential. Correspondingly, the change in pH and CO_2 concentration is also small in the solution without the pyridinium mediator (Fig. S12B & C). The results in Fig. S12 indicate that the faradaic current in Fig. 3 predominantly arises from the reduction of the pyridinium mediators, with concomitant pH increase and CO_2 capture being directly associated with this redox process rather than HER.



Carbon capture/release experiments in a flow cell

From Fig. 3, it can be concluded that BzSP shows the best performance in the CO_2 capture/release test. As the next step, we scaled up the synthesis of this champion mediator to a 20 g scale (see SI) and tested its energy efficiency for the CO_2 capture/release in a more commercially relevant flow cell. The schematic diagram of the flow cell setup is displayed in Fig. 4A. The cell was assembled with a Nafion 117 membrane and 4 cm^2 carbon papers (Sigracet 22AA) as the working and counter electrodes. The negolyte contained 25 mL of 0.1 M pyridinium mediator in 1 M KNO_3 , and the posolyte contained 40 mL of 0.1 M $\text{K}_3\text{Fe}(\text{CN})_6$ and 0.2 M $\text{K}_4\text{Fe}(\text{CN})_6$. The negolyte was continuously purged with a $\text{CO}_2 : \text{N}_2$ mixture (10 : 90, v/v), and the pH of the negolyte was monitored by a pH sensor. Two peristaltic pumps were used to circulate the negolyte and posolyte into the cell during the test.

Fig. 4B–E plots the results of pH-swing CO_2 capture/release in the flow cell configuration. The redox cycling protocol applied reduction and oxidation current of $\pm 20 \text{ mA cm}^{-2}$, respectively (Fig. 4C), with both stages maintained for 30 minutes to ensure equivalent total charge between the redox processes. In the first and second cycles, during the reduction stage, the cell potential was around -1.0 V (Fig. 4B), and the pH

of the negolyte rose from 3.6 to 8.5 (Fig. 4D) concomitant with CO_2 concentration dropping from 10% to 2.9% (Fig. 4E), demonstrating CO_2 capture through proton consumption. A subsequent equilibration period at OCP allowed for further CO_2 uptake, as shown by a gradual decrease in pH to 7.2. In the reoxidation stage, the cell potential was between 1.4 and 1.6 V, triggering a decrease in pH to 2.3 and an increase in CO_2 concentration to 25.2%, thereby confirming CO_2 release through proton regeneration.¹³

In the CO_2 concentration plot, the CO_2 release peak is narrower than the capture peak, and the maximum CO_2 concentration change in the oxidation stage is larger than that observed in the reduction stage. These results indicate that the rate of CO_2 release is faster than the rate of CO_2 capture. This difference arises because CO_2 capture is controlled by CO_2 absorption kinetics, while CO_2 release is constrained by the applied current density.¹³

At the end of the second cycle, the reoxidation potential exhibits a sudden increase from 1.7 V to 1.9 V. This increase suggests that BzSP may be depleted within the electrolyte. Subsequently, during the third cycle, the reduction potential decreases to -1.6 V while the oxidation potential increases further to 1.9 V. The elevated cell potential indicates that water splitting, which requires higher energy than BzSP reduction, becomes the dominant reaction. The depletion of BzSP during cycling is further supported by post-mortem CV analysis from H-cell capture/release tests, where the redox peaks of BzSP greatly diminish after three cycles (Fig. S13). These results demonstrate that BzSP remains stable for approximately 16 hours, corresponding to two full cycles. The pH of the negolyte at the end of the third cycle is higher than that measured at the end of the first and second cycles. This increase results from BzSP degradation reactions, which consume H^+ ions (see the next section for mechanistic studies of BzSP reduction).

The theoretical CO_2 capture capacity of the BzSP solution can be calculated as:

$$C = nc_{\text{BzSP}}V \quad (1)$$

where n , c_{BzSP} , V are the number of electrons transferred per BzSP molecule during reduction/oxidation ($n = 1$), concentration of BzSP, and volume of negolyte, respectively. Following 30 minutes of reduction at 20 mA cm^{-2} , approximately 60% of the theoretical BzSP capacity was reduced. The amount of CO_2 captured/released by BzSP can be calculated using the area of peaks in the CO_2 concentration plot (Fig. 4E). The CO_2 capture/release efficiency (CE) can be determined as the ratio between the moles of CO_2 captured/released and moles of electrons transferred as:

$$\text{CE} = \frac{n_{\text{CO}_2}}{n_e} \times 100\% = \frac{vpFA_{\text{CO}_2}}{RTI} \times 100\% \quad (2)$$

where v , p , F , A_{CO_2} , R , T , I , t are the flow rate of effluent gas, pressure, Faraday constant, area of the CO_2 peak, ideal gas constant, temperature, current, and time, respectively. The energy efficiency (EE) of the flow cell can also be calculated as:

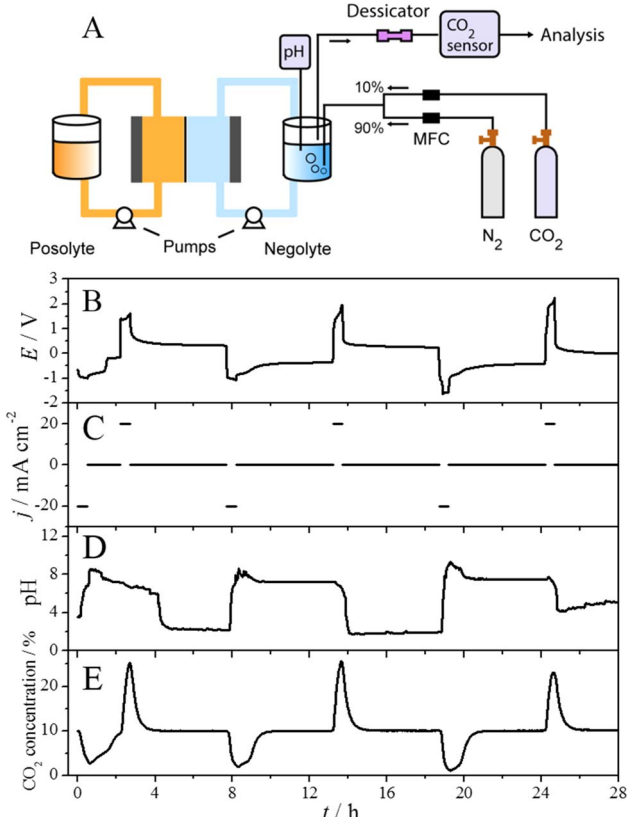


Fig. 4 (A) Schematic diagram of the flow cell system used in the pH-swing CO_2 capture/release test. (B–E) Variation of the cell potential (B), current density of WE (C), pH of negolyte (D) and CO_2 concentration (E) as a function of time during the CO_2 capture/release test.



Table 1 CO_2 capture/release efficiency, energy efficiency and CO_2 capture/release ratio using 0.1 M BzSP in the flow cell at a current density of 20 mA cm⁻²

	CO_2 capture/release efficiency/%	Energy efficiency/kJ mol $_{\text{CO}_2}$ ⁻¹	CO_2 capture/release ratio/%
Reduction cycle 1	90	102	88
Oxidation cycle 1	102	136	
Reduction cycle 2	89	108	84
Oxidation cycle 2	107	136	
Reduction cycle 3	94	143	98
Oxidation cycle 3	95	176	

$$\text{EE} = \frac{W}{n_{\text{CO}_2}} = \frac{EIt}{vpFA_{\text{CO}_2}/RT} \quad (3)$$

The CO_2 capture/release ratio (C/R) in one reduction–oxidation cycle is determined as:

$$C/R = \frac{A_{\text{CO}_2\text{-re}}}{A_{\text{CO}_2\text{-ox}}} \quad (4)$$

where $A_{\text{CO}_2\text{-re}}$ and $A_{\text{CO}_2\text{-ox}}$ are the area of the CO_2 peak in the reduction and oxidation steps, respectively.

During the first two cycles, the CO_2 capture/release efficiency is approximately 90% in the reduction stage and surpasses 100% in the oxidation stage (Table 1). The high efficiency in the oxidation stage may result from faster kinetics during CO_2

release. In the third cycle, where water splitting occurs, the efficiency of the reduction and oxidation stages becomes similar. In the reduction stage of the first two cycles, the energy efficiency of CO_2 capture is 102 kJ mol $_{\text{CO}_2}$ ⁻¹, and in the oxidation stage, the energy efficiency of CO_2 release is 136 kJ mol $_{\text{CO}_2}$ ⁻¹. For the third cycle, the energy input increases for both stages due to the higher energy demand of water splitting compared to BzSP reduction and reoxidation.

The performance and energy efficiency of BzSP is compared with other reported redox mediators in Table S2. The reduction potential and CO_2 capture energy efficiency of BzSP are competitive with state-of-the-art redox mediators.^{9,11,13,16} However, a significant energy cost is incurred during the oxidation stage, resulting in an overall energy efficiency that is

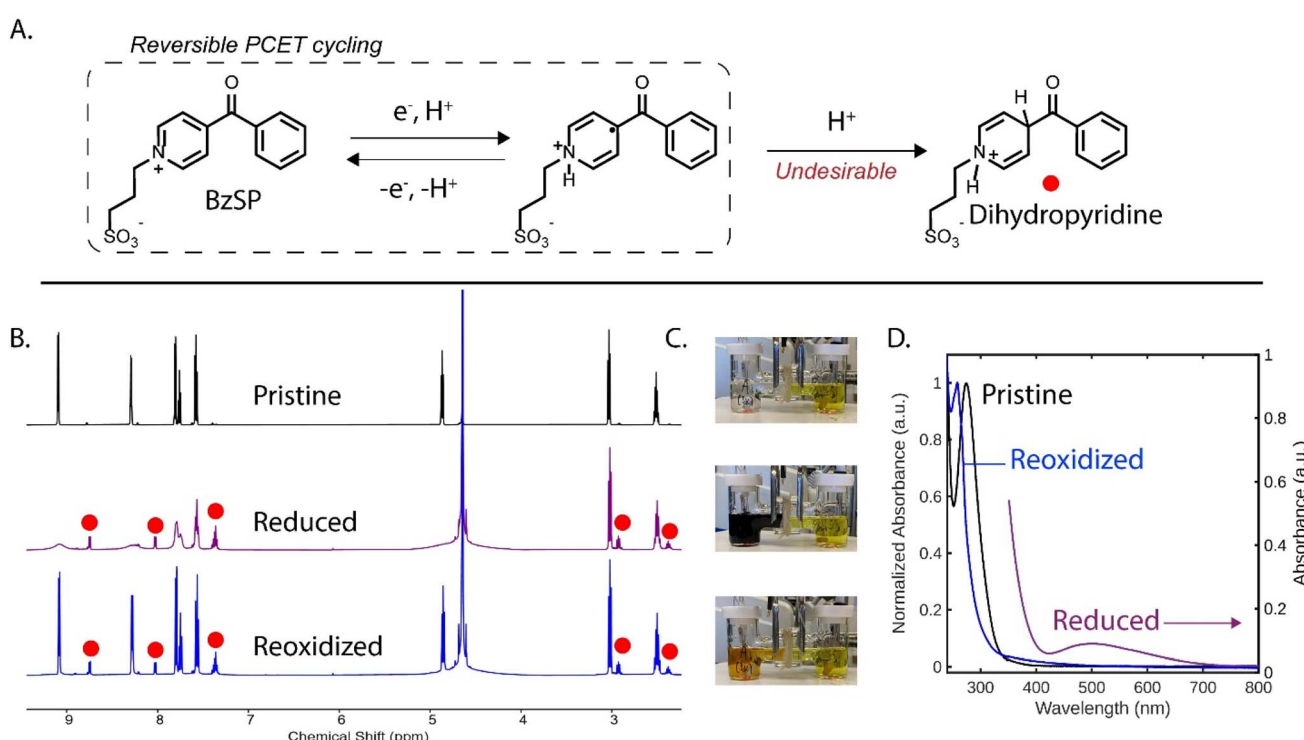


Fig. 5 (A) Mechanism for BzSP-mediated CO_2 capture, including degradation reaction to dihydropyridine. (B) ^1H NMR spectra (D_2O , 500 MHz) of 0.1 M BzSP in 1 M KNO_3 at different stages of the cycling process. (C) Photographs of the BzSP solution (left compartment) at each stage. (D) UV-visible absorption spectra at each stage. The pristine and reoxidized spectra are normalized, while the reduced spectrum is not. A large absorbance below 400 nm in the reduced spectrum is due to the high concentration of active species, which is necessary to observe the radical band.

currently higher than literature values for other mediators. To enhance the viability of our system, we are actively optimizing the oxidative process to improve its energy efficiency.

Mechanistic studies

To gain insight into the mechanism of BzSP, we carried out a similar CO₂ capture/release experiment using D₂O as the electrolyte solvent, thus enabling ¹H NMR analysis of the mediator at each stage of the process (Fig. 5B). Initially, the BzSP mediator is in its pristine state and its NMR peaks are aligned with those found in pure D₂O. Following reduction, a broadening of the aromatic peaks is observed, consistent with the formation of radicals. This is further supported by UV-vis spectroscopy of the deep purple reduced capture solution (Fig. 5C), which shows a broad band centered at 500 nm (Fig. 5D).²⁷ Exposure of this solution to CO₂ leads to a new peak at 160 ppm in the ¹³C NMR spectrum, which is attributed to HCO₃⁻, thus confirming successful sequestration of CO₂ (Fig. S14).

The NMR analysis is particularly useful for monitoring degradation. During reduction, small side peaks emerge in both the aromatic and aliphatic regions, indicating the formation of a new product with a very similar structure to BzSP (Fig. 5B). These peaks are still observed following oxidation and therefore represent a small loss of mediator over one capture/release cycle (approximately 11%). From mass spectrometry (Fig. S15) and further NMR studies (Fig. S16), the product is assigned as the dihydropyridine derivative of BzSP (Fig. 5A), which is consistent with previous work on pyridinium mediators.¹⁹ Interestingly, the dihydropyridine signal does not increase following the oxidation step, implying that the degradation primarily occurs in the early stage of reduction, where some of the mediator is in radical form and pH is relatively low. Thus, improving the radicals' stability to H⁺-induced degradation is crucial to improving the cycle life of this CO₂ capture system. This has been achieved in organic solvents through careful design of the N- and 4-substituents.²⁸

An experiment in D₂O was also carried out for AcSP to understand its poor performance. Following reduction, the acetyl CH₃ signal is absent from the solution's ¹H NMR spectrum, indicating enolization and subsequent proton exchange with the solvent (Fig. S17), which is consistent with previous work.¹⁹ The ability of AcSP to enolize means that it is susceptible to aldol reactions, and therefore has more available degradation pathways than BzSP.

Conclusions

Three water-soluble pyridinium-based redox mediators (BzM, BzSP, AcSP) have been synthesized and evaluated for electrochemical pH-swing CO₂ capture/release, and we have identified structure–performance relationships, degradation mechanisms, and practical limitations. These molecules show reversible redox behavior and can electrochemically induce pH-swings, thus opening the door to CO₂ capture. In H-cell tests, BzSP demonstrates optimal CO₂ capture capacity, evidenced by

higher reduction currents, larger pH swings, and greater CO₂ concentration changes than AcSP and BzM. In a flow cell setup, BzSP exhibits stable operation for two full cycles (~16 h), achieving ~90% CO₂ capture efficiency and ~100% CO₂ release efficiency. The energy requirement for CO₂ capture is 102 kJ mol_{CO₂}⁻¹, however, CO₂ release during oxidation requires significantly more energy (136 kJ mol_{CO₂}⁻¹), highlighting a key area for optimization. Degradation of the molecules through an acid-induced pathway was observed, which limits the mediator lifetime. Future work will aim to lower the energetic input of the oxidation stage, to improve the cycling life through rational molecular engineering, and to carry out experiments with more practically relevant gas streams, which include oxygen and impurities such as SO_x and NO_x. Overall, this study establishes that the acylpyridinium family is suitable for electrochemically mediated CO₂ capture and paves the way for the development of new pH-swing redox mediators.

Author contributions

EG, DS, PK, and SC conceived the project. EG and JTL carried out the synthesis. ZS carried out FTIR while EG and JTL carried out all other chemical characterization. EG, JTL, ZS, SC, and AL carried out electrochemical studies. AW helped with system design. ZS and SC carried out long-term CO₂ capture/release tests and analysis. EG and ZS drafted the manuscript and all authors contributed to revision. DS, PK, and SC supervised the project.

Conflicts of interest

There are no conflicts to declare.

Data availability

The authors confirm that the data supporting the findings of this study are available within the article and/or its SI. Supplementary information is available. See DOI: <https://doi.org/10.1039/d5sc04731e>.

Acknowledgements

We gratefully acknowledge financial support provided by the Natural Sciences and Engineering Research Council of Canada (NSERC) Discovery Grants Program (RGPIN-2022-04319), the National Research Council (NRC) of Canada's Collaborative Centre for Green Energy Materials (CC-GEM), and the Materials for Clean Fuels (MCF) Challenge Program at the NRC. EG and JTL are grateful for graduate scholarships from NSERC.

References

- 1 J. M. Barlow, L. E. Clarke, Z. Zhang, D. Bím, K. M. Ripley, A. Zito, F. R. Brushett, A. N. Alexandrova and J. Y. Yang, Molecular Design of Redox Carriers for Electrochemical CO₂ Capture and Concentration, *Chem. Soc. Rev.*, 2022, **51**(20), 8415–8433, DOI: [10.1039/D2CS00367H](https://doi.org/10.1039/D2CS00367H).



2 A. Ozden, CO₂ Capture *via* Electrochemical pH-Mediated Systems, *ACS Energy Lett.*, 2025, **10**, 1550–1576, DOI: [10.1021/acsenergylett.5c00200](https://doi.org/10.1021/acsenergylett.5c00200).

3 S. E. Renfrew, D. E. Starr and P. Strasser, Electrochemical Approaches toward CO₂ Capture and Concentration, *ACS Catal.*, 2020, **10**(21), 13058–13074, DOI: [10.1021/acscatal.0c03639](https://doi.org/10.1021/acscatal.0c03639).

4 M. Rahimi, A. Khurram, T. A. Hatton and B. Gallant, Electrochemical Carbon Capture Processes for Mitigation of CO₂ Emissions, *Chem. Soc. Rev.*, 2022, **51**(20), 8676–8695, DOI: [10.1039/D2CS00443G](https://doi.org/10.1039/D2CS00443G).

5 P. Singh, J. H. Rheinhardt, J. Z. Olson, P. Tarakeshwar, V. Mujica and D. A. Buttry, Electrochemical Capture and Release of Carbon Dioxide Using a Disulfide-Thiocarbonate Redox Cycle, *J. Am. Chem. Soc.*, 2017, **139**(3), 1033–1036, DOI: [10.1021/jacs.6b10806](https://doi.org/10.1021/jacs.6b10806).

6 R. Ranjan, J. Olson, P. Singh, E. D. Lorance, D. A. Buttry and I. R. Gould, Reversible Electrochemical Trapping of Carbon Dioxide Using 4,4'-Bipyridine That Does Not Require Thermal Activation, *J. Phys. Chem. Lett.*, 2015, **6**(24), 4943–4946, DOI: [10.1021/acs.jpclett.5b02220](https://doi.org/10.1021/acs.jpclett.5b02220).

7 S. Voskian and T. Alan Hatton, Faradaic Electro-Swing Reactive Adsorption for CO₂ Capture, *Energy Environ. Sci.*, 2019, **12**(12), 3530–3547, DOI: [10.1039/C9EE02412C](https://doi.org/10.1039/C9EE02412C).

8 H. Seo, M. P. Nitzsche and T. A. Hatton, Redox-Mediated pH Swing Systems for Electrochemical Carbon Capture, *Acc. Chem. Res.*, 2023, **56**(22), 3153–3164, DOI: [10.1021/acs.accounts.3c00430](https://doi.org/10.1021/acs.accounts.3c00430).

9 Y. Jing, K. Amini, D. Xi, S. Jin, A. M. Alfaraidi, E. F. Kerr, R. G. Gordon and M. J. Aziz, Electrochemically Induced CO₂ Capture Enabled by Aqueous Quinone Flow Chemistry, *ACS Energy Lett.*, 2024, **9**(7), 3526–3535, DOI: [10.1021/acsenergylett.4c01235](https://doi.org/10.1021/acsenergylett.4c01235).

10 C. Huang, C. Liu, K. Wu, H. Yue, S. Tang, H. Lu and B. Liang, CO₂ Capture from Flue Gas Using an Electrochemically Reversible Hydroquinone/Quinone Solution, *Energy Fuels*, 2019, **33**(4), 3380–3389, DOI: [10.1021/acs.energyfuels.8b04419](https://doi.org/10.1021/acs.energyfuels.8b04419).

11 S. Jin, M. Wu, R. G. Gordon, M. J. Aziz and D. G. Kwabi, pH Swing Cycle for CO₂ Capture Electrochemically Driven through Proton-Coupled Electron Transfer, *Energy Environ. Sci.*, 2020, **13**(10), 3706–3722, DOI: [10.1039/D0EE01834A](https://doi.org/10.1039/D0EE01834A).

12 H. Xie, Y. Wu, T. Liu, F. Wang, B. Chen and B. Liang, Low-Energy-Consumption Electrochemical CO₂ Capture Driven by Biomimetic Phenazine Derivatives Redox Medium, *Appl. Energy*, 2020, **259**, 114119, DOI: [10.1016/j.apenergy.2019.114119](https://doi.org/10.1016/j.apenergy.2019.114119).

13 S. Pang, S. Jin, F. Yang, M. Alberts, L. Li, D. Xi, R. G. Gordon, P. Wang, M. J. Aziz and Y. Ji, A Phenazine-Based High-Capacity and High-Stability Electrochemical CO₂ Capture Cell with Coupled Electricity Storage, *Nat. Energy*, 2023, **8**(10), 1126–1136, DOI: [10.1038/s41560-023-01347-z](https://doi.org/10.1038/s41560-023-01347-z).

14 H. Seo and T. A. Hatton, Electrochemical Direct Air Capture of CO₂ Using Neutral Red as Reversible Redox-Active Material, *Nat. Commun.*, 2023, **14**(1), 313, DOI: [10.1038/s41467-023-35866-w](https://doi.org/10.1038/s41467-023-35866-w).

15 S. Jin, M. Wu, Y. Jing, R. G. Gordon and M. J. Aziz, Low Energy Carbon Capture *via* Electrochemically Induced pH Swing with Electrochemical Rebalancing, *Nat. Commun.*, 2022, **13**(1), 1–11, DOI: [10.1038/s41467-022-29791-7](https://doi.org/10.1038/s41467-022-29791-7).

16 H. Seo, M. Rahimi and T. A. Hatton, Electrochemical Carbon Dioxide Capture and Release with a Redox-Active Amine, *J. Am. Chem. Soc.*, 2022, **144**(5), 2164–2170, DOI: [10.1021/jacs.1c10656](https://doi.org/10.1021/jacs.1c10656).

17 H. Xie, W. Jiang, T. Liu, Y. Wu, Y. Wang, B. Chen, D. Niu and B. Liang, Low-Energy Electrochemical Carbon Dioxide Capture Based on a Biological Redox Proton Carrier, *Cell Rep. Phys. Sci.*, 2020, **1**(5), 100046, DOI: [10.1016/j.xcrp.2020.100046](https://doi.org/10.1016/j.xcrp.2020.100046).

18 C. J. Li, J. W. Ziller, J. M. Barlow and J. Y. Yang, Aqueous Electrochemical and pH Studies of Redox-Active Guanidino Functionalized Aromatics for CO₂ Capture, *ACS Org. Inorg. Au*, 2024, **4**(4), 387–394, DOI: [10.1021/acs.orginorgau.3c00066](https://doi.org/10.1021/acs.orginorgau.3c00066).

19 C. S. Sevov, K. H. Hendriks and M. S. Sanford, Low-Potential Pyridinium Anolyte for Aqueous Redox Flow Batteries, *J. Phys. Chem. C*, 2017, **121**(44), 24376–24380, DOI: [10.1021/acs.jpcc.7b06247](https://doi.org/10.1021/acs.jpcc.7b06247).

20 A. Harriman, G. R. Millward, P. Neta, M. C. Richoux and J. M. Thomas, Interfacial Electron-Transfer Reactions between Platinum Colloids and Reducing Radicals in Aqueous Solution, *J. Phys. Chem.*, 1988, **92**(5), 1286–1290, DOI: [10.1021/j100316a054](https://doi.org/10.1021/j100316a054).

21 D. R. Weinberg, C. J. Gagliardi, J. F. Hull, C. F. Murphy, C. A. Kent, B. C. Westlake, A. Paul, D. H. Ess, D. G. McCafferty and T. J. Meyer, Proton-Coupled Electron Transfer, *Chem. Rev.*, 2012, **112**(7), 4016–4093, DOI: [10.1021/cr200177j](https://doi.org/10.1021/cr200177j).

22 C. DeBruler, B. Hu, J. Moss, J. Luo and T. L. Liu, A Sulfonate-Functionalized Viologen Enabling Neutral Cation Exchange, Aqueous Organic Redox Flow Batteries toward Renewable Energy Storage, *ACS Energy Lett.*, 2018, **3**(3), 663–668, DOI: [10.1021/acsenergylett.7b01302](https://doi.org/10.1021/acsenergylett.7b01302).

23 R. Rubio-Presa, L. Lubián, M. Borlaf, E. Ventosa and R. Sanz, Addressing Practical Use of Viologen-Derivatives in Redox Flow Batteries through Molecular Engineering, *ACS Mater. Lett.*, 2023, **5**(3), 798–802, DOI: [10.1021/acs.materialslett.2c01105](https://doi.org/10.1021/acs.materialslett.2c01105).

24 E. Grignon, J. T. Liu, Y. F. Tan, Y. Cao, A. Aspuru-Guzik and D. S. Seferos, Highly Water-Soluble Polyether-Based Viologen Negolytes for Aqueous Redox-Flow Batteries, *J. Am. Chem. Soc.*, 2025, **147**(6), 5071–5079, DOI: [10.1021/jacs.4c14969](https://doi.org/10.1021/jacs.4c14969).

25 A. Debiais, C. Lai, T. Boulanger, G. Reynard, L. Hamlet, S. Généreux, M. Vaillancourt, R. Iftimie, H. Lebel and D. Rochefort, Highly Soluble Viologen-PEG Conjugates for Aqueous Organic Redox Flow Batteries, *ACS Appl. Energy Mater.*, 2025, **8**(1), 181–193, DOI: [10.1021/acsaelm.4c02259](https://doi.org/10.1021/acsaelm.4c02259).

26 P. T. Sullivan, H. Liu, X.-L. Lv, S. Jin, W. Li and D. Feng,



Viologen Hydrothermal Synthesis and Structure–Property Relationships for Redox Flow Battery Optimization, *Adv. Energy Mater.*, 2023, 13(34), 2203919, DOI: [10.1002/aenm.202203919](https://doi.org/10.1002/aenm.202203919).

27 E. M. Kosower, Stable Pyridinyl Radicals, in *Preparative Organic Chemistry*, Springer, Berlin, 1983, pp. 117–162, DOI: [10.1007/3-540-12396-2_7](https://doi.org/10.1007/3-540-12396-2_7).

28 C. S. Sevov, D. P. Hickey, M. E. Cook, S. G. Robinson, S. Barnett, S. D. Minteer, M. S. Sigman and M. S. Sanford, Physical Organic Approach to Persistent, Cyclable, Low-Potential Electrolytes for Flow Battery Applications, *J. Am. Chem. Soc.*, 2017, 139(8), 2924–2927, DOI: [10.1021/jacs.7b00147](https://doi.org/10.1021/jacs.7b00147).

